

# Shack Hartmann wave-front measurement with a large F-number plastic microlens array

Geun Young Yoon, Takahisa Jitsuno, Masahiro Nakatsuka, and Sadao Nakai

A new plastic microlens array, consisting of 900 lenslets, has been developed for the Shack Hartmann wave-front sensor. The individual lens is  $300\ \mu\text{m} \times 300\ \mu\text{m}$  and has a focal length of 10 mm, which provides the same focal size,  $60\ \mu\text{m}$  in diameter, with a constant peak intensity. One can improve the wave-front measurement accuracy by reducing the spot centroiding error by averaging a few frame memories of an image processor. A deformable mirror for testing the wave-front sensor gives an appropriate defocus and astigmatism, and the laser wave front is measured with a Shack Hartmann wave-front sensor. The measurement accuracy and reproducibility of our wave-front sensor are better than  $\lambda/20$  and  $\lambda/50$  ( $\lambda = 632.8\ \text{nm}$ ), respectively, in rms.

*Key words:* Plastic microlens array, Shack Hartmann wave-front sensor, deformable mirror.  
© 1996 Optical Society of America

## 1. Introduction

In direct-drive laser fusion the fusion reaction takes place in compressed deuterium and tritium fuel at a high temperature and in high density under irradiation of a high-power laser onto the fuel pellet target.<sup>1</sup> The improvement in laser irradiation uniformity of a spherical target is necessary for higher efficiency in the fusion reaction.

In the laser system used for this purpose, large optical devices of several tens of centimeters are used to avoid laser-induced damage.<sup>2</sup> However, large optical devices are difficult to fabricate with good surface accuracy and are distorted by their weight in the oblique arrangement. The laser wave-front aberration is caused by a phase error in the optical devices and thermal distortion from a high repetition shot that degrades the laser-beam quality, which causes deterioration in irradiation uniformity.

To control the laser wave front, we developed an active optical system that consists of a wave-front measurement and wave-front compensation system.<sup>3</sup> As the wave-front measurement method, we adopted the Shack Hartmann wave-front sensor (SHWS), which is a modification of the classic method of testing large optical devices, such as large telescope

optical devices. This measurement system is known as the Hartmann test.<sup>4,5</sup> The SHWS has the following advantages for wave front measuring an incident laser beam with a large aperture. First, common interferometric methods such as the Fizeau-type interferometer require a large aperture beam and a reference plane mirror of good quality. However, with the SHWS, one can produce a reference beam easily by introducing a pinhole into the focal point of reducing optics or a reference plane mirror to measure a reflective surface. Second, because wave-front distortion is in inverse proportion to the magnifying power of the beam aperture, the larger the beam aperture becomes, the higher the measurement accuracy that can be obtained. Third, because the SHWS has a local wave-front slope, one can achieve a wave-front correction directly by local wave-front control, using individual actuators on a deformable mirror.

In this paper, first we describe the SHWS principle. In Section 3 the development and evaluation of a plastic microlens array with a long focal length are presented. In Section 4 we propose a method for reducing the centroiding error of the image spot, and the experimental results of the SHWS performance are reported in Section 5.

## 2. Requirements for the SHWS

The SHWS has been used as a wave-front measuring method of an aberrated large-aperture beam. The Hartmann wave-front sensor measures the wave-front aberration from the local wave-front slope

---

The authors are with the Institute of Laser Engineering, Osaka University, 2-6 Yamada-oka, Suita, Osaka 565, Japan.

Received 2 February 1995; revised manuscript received 10 August 1995.

0003-6935/96/010188-05\$06.00/0

© 1996 Optical Society of America

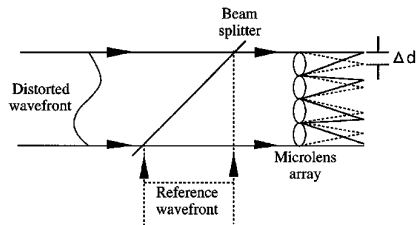


Fig. 1. Schematic of the SHWS.

divided by the Hartmann plate with many small holes. The Hartmann wave-front sensor was developed to measure large telescope optical devices; it was improved and became the SHWS. Figure 1 shows schematically the SHWS principle. The incident laser beam is divided into a number of beamlets by a two-dimensional microlens array. Each lenslet provides a separate focus, and the centroid position of each spot is displaced by a local wave-front aberration between the reference and distorted beams. Because each local wave-front slope corresponds to wave-front distortion, the whole beam wave front can be reconstructed by integration of local wave-front slope  $\theta$ :

$$\theta = \Delta d / f, \quad (1)$$

where  $\Delta d$  is the displacement of the spot centroid and  $f$  is the focal length of the microlens.

The microlens array is one of the most important elements of the SHWS. A small-size, long-focal-length microlens array must be developed in the SHWS to improve measurement accuracy. However, fabrication of the microlens with a large F number and nearly diffraction-limited specification is difficult and expensive.

### 3. Development and Evaluation of a Plastic Microlens Array

We have developed a long-focal-length microlens array made of optical plastic material. The optical plastic as the microlens-array material is easier to manufacture, less expensive, and has a higher shock strength than optical glass. The lens array is manu-

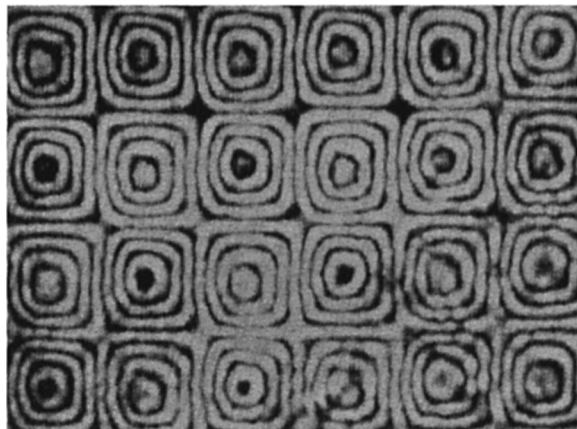


Fig. 2. Microscopic interferogram of the microlens array.

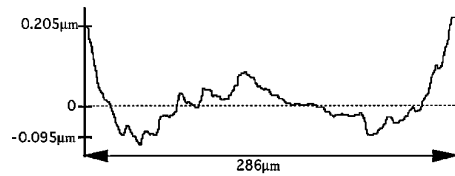


Fig. 3. One-dimensional surface profile by the difference in the ideal lens shape.

factured by spouting optical plastic material into a metal mold obtained by successively stamping a stainless-steel ball. This technique is inexpensive and suitable for mass production of a microlens array<sup>6</sup> or an aspherical lens if the metal mold is made precisely.

Figure 2 shows the microscopic interferogram of the transmission wave front of a microlens array. The rectangular interference fringe on the periphery of the lenslet is caused by the stamping process with the stainless-steel ball. The rectangular fringe indicates that the lenslet has optical aberrations. The spot pattern, however, is not affected by this aberration because the aberrated components are defocused out of the central lobe as shown in Fig. 4. The effective area of each lenslet is  $\sim 75\%$  of the lenslet, which is estimated from the intensity distribution of the spot pattern. The defocused components are observed on a pedestal of the pattern and are easily removed during the calculation process of the spot center. Figure 3 shows a discrepancy in the one-dimensional surface profile of a lenslet with respect to the designed surface profile. The difference in the designed lens shape was less than  $0.1 \mu\text{m}$  (2%) for a maximum stamping depth of  $4.5 \mu\text{m}$ .

The individual lens (there are 900 in our microlens array) has a rectangular shape of  $300 \mu\text{m} \times 300 \mu\text{m}$  and a focal length of 10 mm. The spot size is  $60 \mu\text{m}$  with a standard deviation,  $\sigma_{\text{spot}} = 1.05 \mu\text{m}$ , as shown in Fig. 4. This spot size is 1.2 times the diffraction

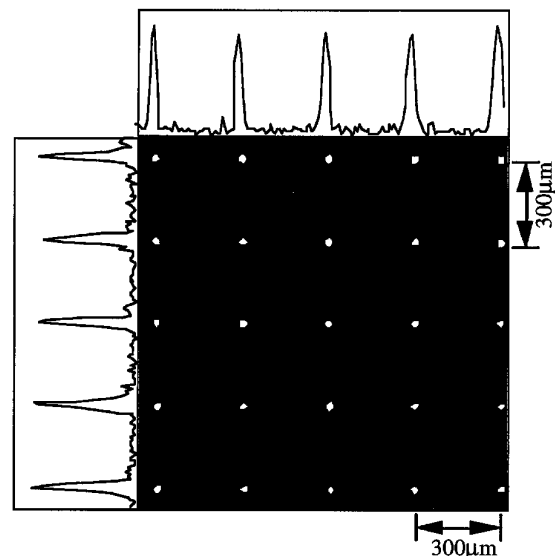


Fig. 4. Spot pattern and intensity distribution.

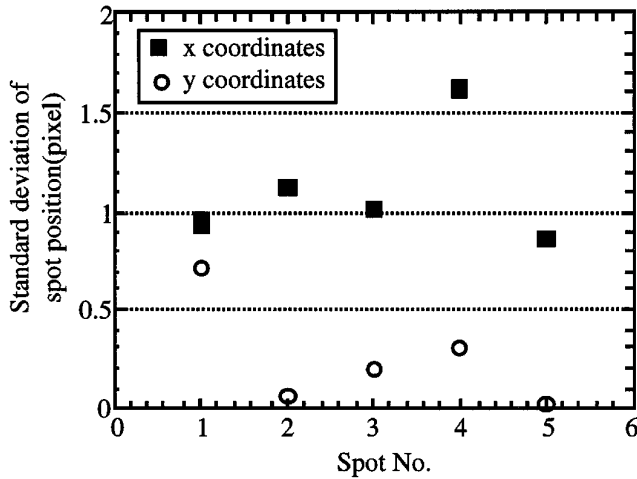


Fig. 5. Centroiding unevenness in the case of one-frame memory only.

limit at a He-Ne laser wavelength, and the peak intensity for each beamlet at the focus is nearly equal. A small fluctuation in the peak intensity between the focal spots does not degrade the measurement accuracy in a process that determines individual center positions of focal spots because only the energy center is calculated.

#### 4. Experiments

##### A. Reduction in the Centroiding Error of Spot Images

The centroid position of an image spot fluctuates from air turbulence, optics vibration, instability in laser intensity, and noise in such detector units as the CCD camera and the image processor.<sup>7</sup> Because the centroid position relates directly to the local wave front, the measurement accuracy is limited by the centroiding error in the image spots.

We have measured the centroiding error and used the method described below to reduce it. The calculation formula of the centroid position  $(x, y)$  of an image spot with optical intensity distribution  $I(x, y)$

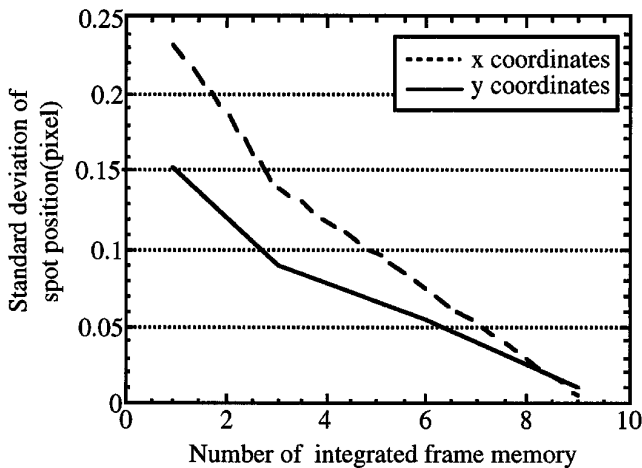


Fig. 6. Reduction in the centroiding error of the spot by integration of frame memories.

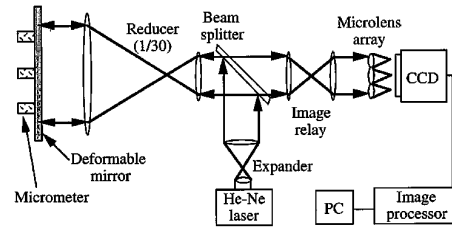


Fig. 7. Schematic of the measurement system of wave-front distortion.

is

$$x = \frac{\sum_{i=1}^m \left( \sum_{j=1}^n x_i I_{i,j} \right)}{\sum_{i=1}^m \left( \sum_{j=1}^n I_{i,j} \right)}, \quad (2)$$

$$y = \frac{\sum_{i=1}^m \left( \sum_{j=1}^n y_i I_{i,j} \right)}{\sum_{i=1}^m \left( \sum_{j=1}^n I_{i,j} \right)}, \quad (3)$$

where  $x, y$  are in pixel dimensions. Figure 5 shows centroiding fluctuations for five spot images between five-frame memory data without integration in the image processor.

To reduce the centroiding error, we have averaged memory data from a few frames by an image processor. Figure 6 shows the error reduction as a function of averaging the number of frames. The standard deviation of the spot center is reduced to  $1/100$  pixel ( $0.1 \mu\text{m}$ ) by integrating nine frame memories, which indicates that the higher the number of the integrated frame memory, the lower becomes the centroiding error of the spot because the errors are caused by a temporal change in the spot image.

The influence of the spot centroiding error on the total wave front is evaluated by the difference in the peak-to-valley (P-V) value of the measured wave-front figure between the SHWS and the Fizeau interferometer. For the only one-frame memory, the measuring error in defocus and astigmatism is  $\sim 1.1\lambda$  and  $1.4\lambda$  for each defocus measurement of  $4.3\lambda$  in P-V and astigmatism of  $6.8\lambda$  in P-V, respectively. On the contrary, for the integration of nine-frame memory data, the error is reduced to  $\sim 0.1\lambda$  and  $0.34\lambda$ , respectively, for the same aberration terms above. The reduction in the spot centroiding error is important in measuring the wave front precisely.

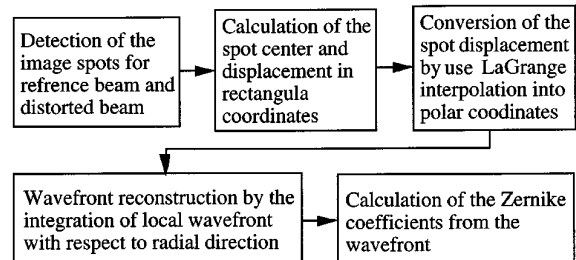


Fig. 8. Block diagram of the algorithm.

## B. Wave-Front Measurement

To evaluate the SHWS performance, we show in Fig. 7 a measurement system that uses a mechanical deformable mirror. The deformable mirror, 185 mm in diameter, can produce appropriate defocus and astigmatism when the mirror surface is pushed with micrometer heads. The use of reducer optics enables the SHWS to have high-measurement accuracy by the enlargement of angular displacement and to test large optical objectives. The He-Ne laser ( $\lambda = 632.8$  nm) is split and magnified by a beam expander and introduced to illuminate a large optical objective. The diameter of reflected light from the deformable mirror (or the reference plane mirror) is reduced, and the surface image of the mirror is relayed onto the plastic microlens array by image-relay optics. The displacements of the spot center between the reference beam by the plane mirror and the aberrated beam by the test mirror are detected by a CCD camera and processed by an image processor and a personal computer. Wave-front reconstruction and expansion of the reconstructed wave front to Zernike circle polynomials<sup>8</sup> are performed by a C-language program.

Figure 8 shows a block diagram of the algorithm for image processing spots and calculating Zernike coefficients.

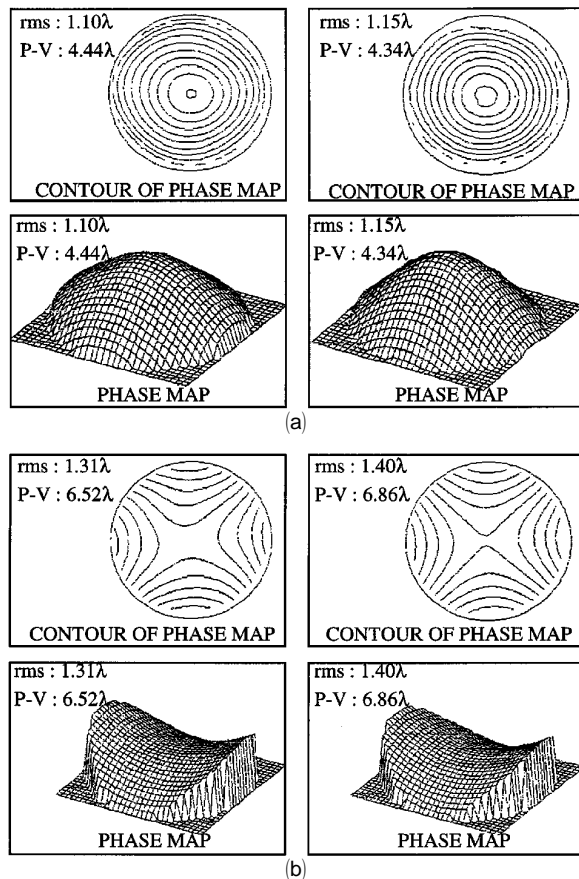


Fig. 9. Measurement results of (a) defocus and (b) astigmatism by (left) the SHWS and (right) the Fizeau interferometer.

Table 1. Comparison of the Lower Zernike Coefficients<sup>a</sup>

Zernike Coefficients	Defocus		Astigmatism	
	SHWS Interferometer	SHWS Interferometer	SHWS Interferometer	SHWS Interferometer
Defocus	1.901	2.077	-0.182	-0.035
Astigmatism 0°	-0.277	-0.237	3.224	3.451
Astigmatism 45°	0.068	0.074	0.243	0.237
Coma <i>x</i>	0.01	0.064	-0.013	-0.036
Coma <i>y</i>	-0.114	-0.115	0.046	0.009
Primary spherical aberration	-0.137	-0.248	0.012	0.003

<sup>a</sup>Units: wavelength (632.8 nm).

## 5. Experimental Results and Discussion

We measured two low-order wave-front aberration terms, defocus and astigmatism, to evaluate the SHWS performance. The wave-front aberration is generated artificially by the deformable mirror and measured by our SHWS and a Fizeau interferometer. Figure 9 shows the measurement results by a three-dimensional phase map and its contour.

Zernike coefficients have been calculated with 6 orders, 27 aberration terms. Table 1 shows a comparison of lower Zernike coefficients (Seidel aberration terms) measured by the SHWS and interferometer.

With this system, because the reference and the distorted beams pass through exactly the same optical path, optical aberrations in the measurement system are eliminated by the reference beam. Therefore the wave front of optical objectives can be measured precisely.

The resolving power of this system is approximately  $\lambda/50$  for a diameter of 130 mm when the stability of spot centroiding is 1/100 pixel (0.1  $\mu\text{m}$ ). The wave-front measurement accuracy of our SHWS is evaluated by a comparative measurement with a Fizeau interferometric method, and it is better than  $\lambda/20$  in rms. The measuring error in lower Zernike coefficients between our SHWS and a Fizeau interferometer is less than  $\lambda/10$  as shown in Table 1. The measurement accuracy can be improved by a microlens array with a longer focal length and a hexagonal arrangement, a larger magnification of the reducing optics, and reduction in the spot centroiding error by integration of a larger number of frame memories.

## 6. Conclusions

The SHWS with a new microlens array has proved to give good results as a method of measuring a laser wave front. The optical system is very simple, and precise optical components are not required with this scheme.

The development of a plastic microlens array with a long focal length has been successful, and we can obtain nearly diffraction-limited spots. By integration of a few frame memories, the centroiding error of the image spot has been reduced remarkably. The position of the spot centroid is stabilized at 1/100

pixel (0.1  $\mu\text{m}$ ), and measurement accuracy is improved.

Consequently the measurement accuracy of the wave front with our SHWS is better than  $\lambda/20$ , which is almost the same as that of the Fizeau interferometer. The measurement error in lower Zernike coefficients between our SHWS and the Fizeau interferometer is less than  $\lambda/10$ . The measurement error is negligible for wave-front control.

#### References and Notes

1. S. Nakai, S. Kahalas, L. I. Rudakov, and S. Witkowski, "Inertial confinement" *Nucl. Fusion* **30**, 1779–1797 (1990).
2. J. L. Emett, W. F. Krupuke, and J. I. Davis, "Laser R&D at the Lawrence Livermore National Laboratory for fusion and isotope separation applications," *IEEE J. Quantum Electron.* **QE-20**, 591–602 (1984).
3. J. W. Hardy, "Adaptive optics—a progress review," in *Active and Adaptive Optical System*, M. A. Ealey, ed., *Proc. Soc. Photo-Opt. Instrum. Eng.* **1542**, 2–17 (1991).
4. R. Shack and B. Platt, *Optical Sciences Newsletter* (University of Arizona, Tucson, Ariz., 1971), Vol. 5, No. 1, p. 15.
5. R. N. Wilson, F. Franza, L. Noethe, and M. Tarenghi, "The ESO off-line telescope testing technique illustrated with results for the MPIA 2.2-m telescope II," in *Proceedings of IAU Colloquium 79: Very Large Telescopes, their Instrumentation and Programs* (Garching, 1984), pp. 119–130.
6. Detailed information can be obtained from Nippon Aspherical Lens Company, 3-2-30 Minami-eguchi, Higashi Yodogawa-ku, Osaka 533, Japan.
7. T. Y. Kane, B. M. Welsh, C. S. Gardner, and L. A. Thompson, "Wavefront detector optimization for laser guided adaptive telescope," in *Active Telescope Systems*, F. J. Roddier, ed., *Proc. Soc. Photo-Opt. Instrum. Eng.* **1114**, 160–171 (1990).
8. M. Born and E. Wolf, *Principles of Optics* (Pergamon, New York, 1970), Chap 9, p. 464.